

## CHAPTER 237

# A Study on Mud Mass Transport under Waves Based on an Empirical Rheology Model

Masahiko Isobe<sup>1</sup> Trien N. Huynh<sup>2</sup> and Akira Watanabe<sup>1</sup>

### Abstract

The rheological properties of mud play an important role in the motion of bed mud due to waves, currents, or combined waves and currents. In this paper, a dynamic rotary shear meter is developed to measure the shear stress in the mud under an arbitrary time history of the shear rate. Kaolinite is tested as an example of bed material and its rheology model is proposed. Another experiment is performed to confirm the predominance of the mud mass transport mode over the suspended mud transport mode in the wave-induced transport. Further experiments examine the role of pressure as an external force of the motion of the bed mud and measure some characteristics of waves on the mud bed. Finally, based on the empirical rheology model, a numerical model is developed to predict the motion of the bed mud, and resulting mud mass transport and wave damping. The calculated mud mass transport velocity and wave height change agree well with measurement.

## 1 Introduction

Muddy coasts represent a type of coastline where the bed material is mainly consists of fine grained, cohesive sediment. Typical muddy coasts are found in China, Vietnam, Indonesia, Bangladesh, Surinam, Brasil, and the United States. Siltation is a problem proper to muddy coasts where the transport mechanism of bed material is quite different from that on sandy coasts. Therefore, it is of great importance to study the transport phenomenon of mud.

The mud transport by waves and currents is separated into two modes: suspended mud transport in the water layer and mud mass transport in the bed. It is expected that the latter mode is quantitatively predominant under a wave action (Shibayama, *et al.*, 1990), but further experimental verification is still needed.

To predict the motion of bed mud and resulting mud mass transport velocity and wave damping, the rheological properties of mud should be given. Rheological models used so far are, for example, elastic, viscous, visco-elastic, visco-plastic, visco-elastic-plastic models (for example, Mei and Liu, 1987; Tsuruya *et al.*, 1987; Sakakiyama and Bijker, 1989; Shibayama *et al.*, 1990). On assuming one of the rheology models, the parameters in the model are determined by using a rotary or oscillatory viscometer, or other similar apparatuses. However, it is necessary to study the relationship between the stress and strain rate under various patterns of motion.

<sup>1</sup>Dept. of Civil Eng., Univ. of Tokyo, Tokyo 113, Japan.

<sup>2</sup>Civil Eng. Div., The Ho Chi Minh Polytechnic Univ., Ho Chi Minh City, Vietnam.

The pressure gradient and bottom friction can be external forces for the motion of bed mud. To develop a numerical model, it is necessary to investigate the dominant external force and to select an appropriate theory to estimate it.

In the following, a series of experiments performed in relation to the above issues are described. Especially in the experiment of the rheological properties of mud, a dynamic rotary shear meter is developed. Based on an empirical rheology model, a one-dimensional numerical model of the motion of bed mud is developed. Calculated mud mass transport velocity and wave height change are compared with measurements.

## 2 Rheological Properties of Mud

In the previous studies, either unidirectional rotary viscometers (Tsuruya *et al.*, 1986; Otsubo and Muraoka, 1988) or oscillatory viscometers (Mehta and Maa, 1986) were used to determine the parameters included in the assumed rheology models. However, it is necessary to examine the general behavior of mud for an arbitrary shear strain or shear rate. For this purpose, a dynamic rotary shear meter is developed in this study.

### 2.1 Dynamic, rotary shear meter

Since muds are tested at mean and high water content ratios, samples cannot stand by themselves. A new apparatus was designed and made as shown in Fig. 1. It consists of two coaxial cylinders of which the outer one is fixed and the inner one can be set in predetermined motions by controlling a stepping motor from a personal computer. The torque which results from the motion of the inner cylinder is measured by strain gages which are attached on an acrylic column supporting the outer cylinder. The gap between two cylinders is made small to ensure a uniform shear stress and the clearance below the inner cylinder is made large to minimize the end effect of the cylinder.

The calibration was performed before each test by static and dynamic loadings. The dynamic loading is performed by a sinusoidal oscillation of a mass and spring system. It was seen that a linear relation is acceptable without a significant error. To check the

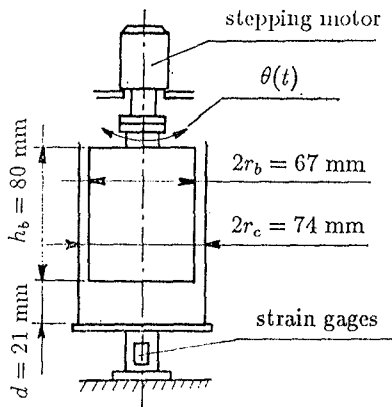


Figure 1: Sketch of the dynamic rotary shear meter.

end effect, a series of tests were done for various depths of mud filled in the gap. By a linear extrapolation of the immersed depth for a null torque, the end effect was found to be equivalent to 1.5 to 2.5 mm which is negligible compared to 70 to 80 mm of the immersed depth.

## 2.2 Experimental condition

### 2.2.1 Patterns of motion

Tests were done for the following patterns of motion.

- 1 ) Pattern S: sinusoidal oscillation which represents wave loading. The amplitude is 0.5 to 8 deg. and the period 1 to 40 s.
- 2 ) Pattern A: linearly varying shear rate in a short duration as shown in Fig. 2. This examines mainly the effect of the shear rate on the shear stress. In the figure,  $T = 10$  to 200 s,  $T_s = 0$  to 20 s, and the rate of change of the shear rate is 0.05 to 1.0 deg./s<sup>2</sup>.
- 3 ) Pattern V: linearly varying shear stress in a long duration. Pattern V is similar to Pattern A but the vertical axis in Fig. 2 is the position in stead of the velocity. The parameter  $T = 100$  to 500 s,  $T_s = 10$  to 200 s, and the rate of change of the position, *i.e.*, the velocity, is 0.01 to 0.2 deg./s.
- 4 ) Pattern SV: combination of constant velocity and oscillation as shown in Fig. 3. This represents the action of combined waves and a current. The velocity is 0.5 to 2 deg./s, the amplitude 1 to 2 deg., and the wave period 1 to 20 s.
- 5 ) Pattern SC: combination of initial shear stress and oscillation as shown in Fig. 4. This examines the effect of creeping.

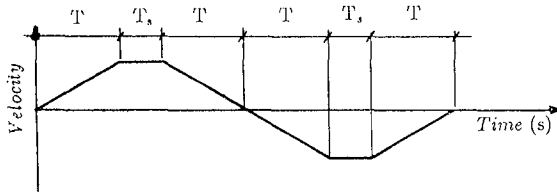


Figure 2: Motion of the inner cylinder (Pattern A).

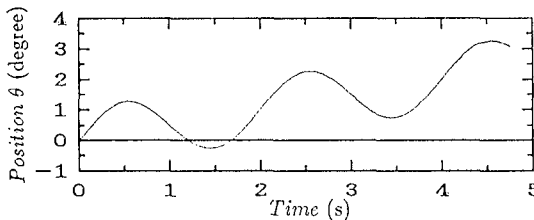


Figure 3: Motion of the inner cylinder (Pattern SV).

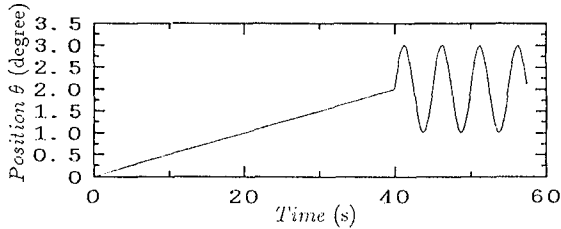


Figure 4: Motion of the inner cylinder (Pattern SC).

### 2.2.2 Mud sample

Commercial kaolin mixed with tap water was used in the experiments. The water content ratio was 126 to 310 %. By the combination of the motion of the shear meter and the water content ratio, the total number of experiments is more than 100.

## 2.3 Experimental result

### 1) Pattern S

Figure 5 shows the relationship between the shear stress and shear rate for sinusoidal oscillations with various wave periods and a fixed amplitude. Curves are not so smooth because the shear rate is obtained by differentiating the displacement numerically. For long wave periods, the stress increases while the shear rate is positive, which implies that the increase of shear strain results in the increase of the shear stress for small shear rates. On the other hand, for short wave periods and therefore for large shear rates, the stress tends to increase with the shear rate but hysteresis loops are formed.

### 2) Pattern A

Figure 6 shows the results for linearly varying shear rates. A hysteresis loop is formed around the origin and linear relations are found for larger magnitudes of shear rates. The path from the maximum to zero shear rate agrees with that for the Bingham fluid. This result is considered to represent general characteristics, while the results for Patterns S and SV represent parts of this path.

### 3) Pattern V

For Pattern V, after the shear rate changes its direction, the shear stress changes abruptly and then gradually approaches to a constant value.

### 4) Pattern SV

Figures 7(a) to (c) represent the results for Pattern SV in which the constant component of shear rate is smaller than, comparative to, and larger than the oscillatory component, respectively. These results can be understood as parts of Figure 6.

### 5) Pattern SC

For Pattern SC, the average stress in one wave period, which is made positive by the initial shear strain, tends to disappear because of the creeping.

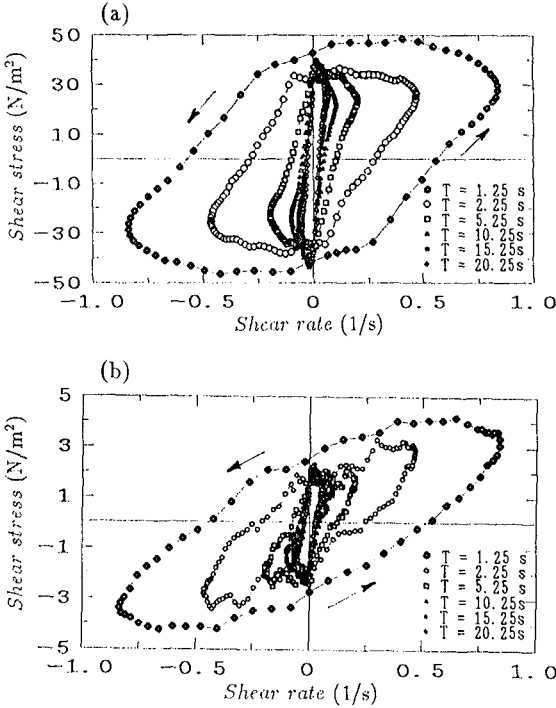


Figure 5: Relationship between shear rate and shear stress (Pattern S).

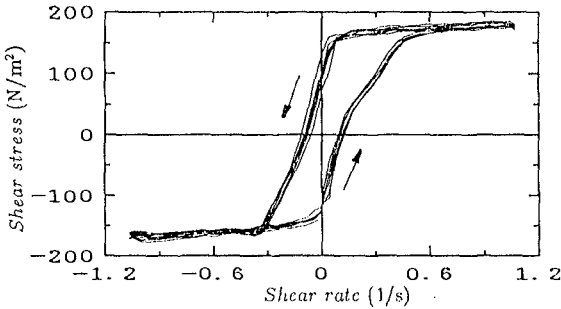


Figure 6: Relationship between shear rate and shear stress (Pattern A).

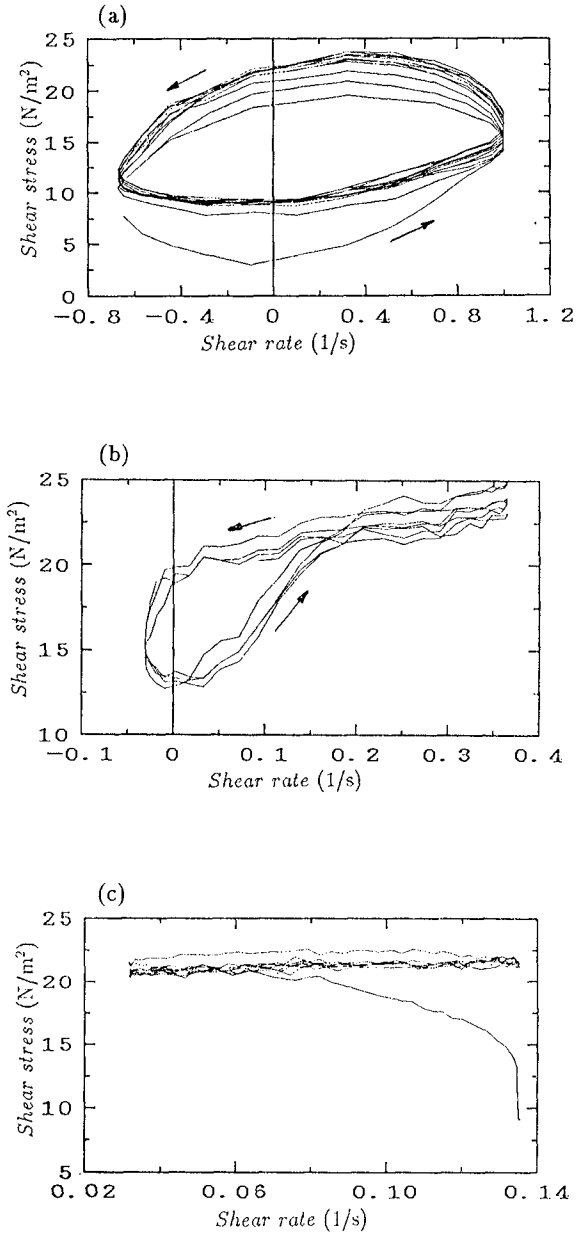


Figure 7: Relationship between shear rate and shear stress (Pattern SV).

2.4 An empirical rheology model

Based on the above experimental results, the following rheology model can be proposed. A backbone curve in Fig. 8 is first introduced:

$$\tau = \begin{cases} \text{sign}(\gamma)\tau_1(|\gamma|/\gamma_c)^n & (|\gamma| \leq \gamma_c) \\ \text{sign}(\gamma)\tau_0 + \mu_1\gamma & (|\gamma| > \gamma_c) \end{cases} \quad (1)$$

When the amplitude of the shear rate is larger than  $\gamma_c$ , the outer path in Fig. 8 is applied:

$$\tau = \begin{cases} \text{sign}(\gamma)\tau_0 + \mu_1\gamma & (|\gamma| \leq \gamma_c, \gamma(d\gamma/dt) \leq 0 \text{ or } |\gamma| > \gamma_c) \\ -\text{sign}(\gamma)\tau_0 + \mu_2\gamma & (|\gamma| \leq \gamma_c, \gamma(d\gamma/dt) > 0) \end{cases} \quad (2)$$

where  $\gamma_c$  is the critical shear rate, and  $\mu_1$  and  $\mu_2$  are viscosities when the magnitude of shear rate is decreasing and increasing, respectively. When the amplitude is smaller than or equal to  $\gamma_c$ , the inner path is applied:

$$\tau = \begin{cases} \text{sign}(\gamma)\tau_{m0} + \mu_1\gamma & (\gamma(d\gamma/dt) \leq 0) \\ -\text{sign}(\gamma)\tau_{m0} + \mu_{m2}\gamma & (\gamma(d\gamma/dt) > 0) \end{cases} \quad (3)$$

where

$$\tau_{m1} = \tau_1(\gamma_{mc}/\gamma_c)^n \quad (4)$$

$$\tau_{m0} = \tau_{m1} - \mu_1\gamma_{mc} \quad (5)$$

$$\mu_{m2} = (\tau_{m1} + \tau_{m0})/\gamma_{mc} \quad (6)$$

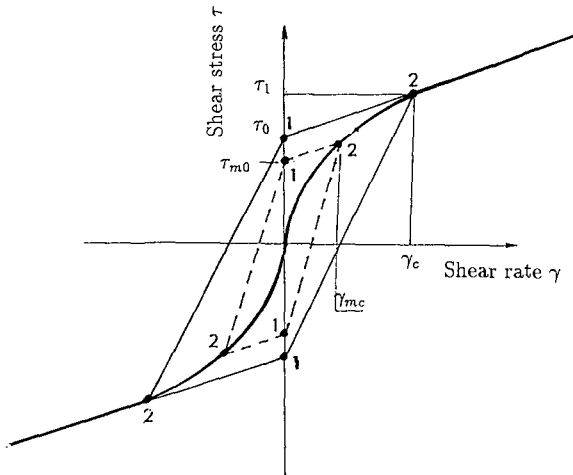


Figure 8: Empirical rheology model.

### 3 Mechanism of Mud Transport

Experiments are done to confirm the predominance of the mud mass transport mode, to measure some properties of waves on mud bed, and to check the importance of the pressure as an external force of the mud mass transport. A wave flume which is 1 m deep, 80 cm wide and 21 m long was used. As shown in Fig. 9, the mud bed was made 12 cm deep and 8 m long.

#### 3.1 Contribution of mud mass transport

A trench of a trapezoidal shape was made at the center of the mud bed and both sides were separated by two walls which prevent the mud mass transport and allow the suspended mud transport. Figure 10 shows the change of bottom configuration due to wave action. As can be seen, the suspended mud transport across the walls is negligible compared to the mud mass transport occurred on seaward and shoreward sides of the walls.

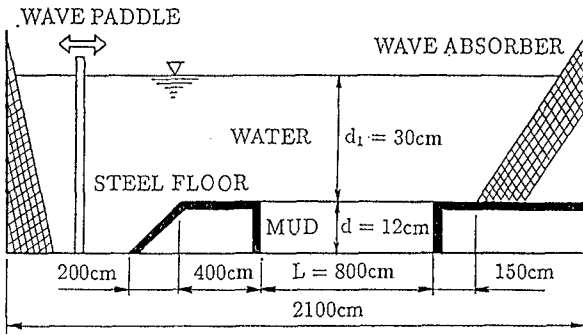


Figure 9: Wave flume and mud bed.

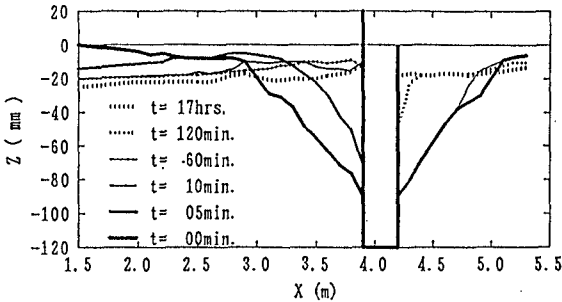


Figure 10: Transformation of trench profile.

### 3.2 Wave properties on the mud bed

#### 3.2.1 wavelength

Figure 11 compares the measured and calculated wavelengths of waves on mud bed. Curves are obtained by the small amplitude wave theory for the depth,  $d_1$ , of the water layer and the total depth,  $d$ , including the depth of mud bed. It is seen that the effect of mud bed on the wavelength is negligible and it is calculated simply from the depth of water.

#### 3.2.2 Pressure in the bed mud

Tsuruya *et al.* (1987) measured the pore pressure in the mud bed. Figure 12 compares the measured and calculated pore pressure. Curves which represent the amplitude of the bottom pressure calculated by the small amplitude wave theory agree well with the measured pore pressure.

### 3.3 Role of pressure as an external force

The gradient of the pressure and shear stress on the bed can be external forces for the bed mud motion. Comparative experiments were done to check the predominance of the pressure. In one experiment, the bed is covered with a nylon sheet which transmits the pressure and at least modifies the shear stress on the bed although it may not cut off completely. The other experiment was done without the cover. Figure 13 compares the wave height decay due to the motion of mud bed with and without the nylon cover. For a wide variety of the incident wave height, the wave height distributions are almost the same, which implies that the pressure gradient due to the wave motion is the dominant external force for the mud motion.

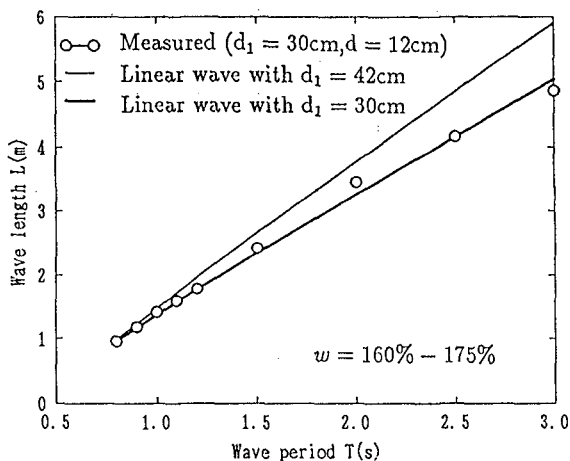


Figure 11: Wavelength of waves on mud bed.

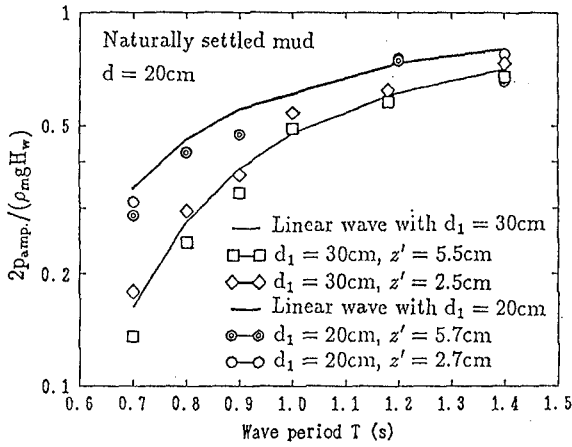


Figure 12: Pore pressure in mud bed.

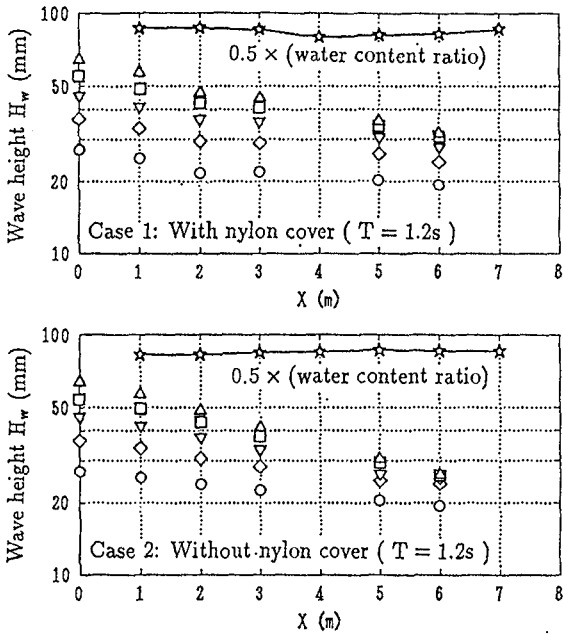


Figure 13: Effect of nylon cover on wave damping.

## 4 Numerical Model of Mud Mass Transport

### 4.1 Oscillatory motion of mud

A numerical model was developed based on the rheology model proposed above.

On assuming that the horizontal length scale is much longer than the vertical scale, the horizontal motion of the bed mud is analyzed as a one-dimensional problem in which the gradient of the pressure is given as the external force. The equation of motion for the velocity,  $u = u(z, t)$ , of the mud is

$$\rho_m \frac{\partial u}{\partial t} = -\frac{\partial p}{\partial x} + \frac{\partial \tau}{\partial z} \quad (7)$$

where  $p$  is the pressure,  $\tau$  the shear stress,  $\rho_m$  the density of the mud,  $x$  and  $z$  the horizontal and vertical coordinates, and  $t$  the time. The pressure is given as the bottom pressure predicted by the small amplitude wave theory. By substituting the shear rate,  $\gamma = \partial u / \partial z$ , into the empirical rheology model proposed above, the shear stress is expressed in terms of  $u$ . Thus, the above equation becomes a closed governing equation for  $u$ . The boundary conditions are the non-slip condition at the bottom of the mud bed and zero shear stress on the bed:

$$u(0, t) = 0 \quad (8)$$

$$\tau(d, t) = 0 \quad (9)$$

Considering the above boundary conditions, the mud layer is divided into  $(N+1/2)$  equal-distance sublayers in discretizing the governing equation. The quantity  $u$  is defined at 0 to  $N$  levels, while  $\tau$  at  $1/2$  to  $N+1/2$  levels. The numerical calculation is continued until a periodic solution is obtained.

## 4.2 Wave damping

The wave damping occurs due to the work done through the shear stress in the mud. The equation of the wave energy is

$$\frac{d}{dx}(EC_g) = -D \quad (10)$$

where  $E = \rho g H^2 / 8$  ( $\rho$ : the density of water,  $g$ : the gravitational acceleration,  $H$ : the wave height) is the wave energy density,  $C_g$  the group velocity, and  $D$  the energy dissipation rate which is estimated by

$$D = \int_0^d \tau \frac{\partial u}{\partial z} dz \quad (11)$$

From Eq. (11), the coefficient,  $D_H$ , of the wave height damping is expressed as

$$D_H \equiv -\frac{1}{H} \frac{dH}{dx} = \frac{1}{2} \frac{D}{EC_g} \quad (12)$$

## 4.3 Mud mass transport

The total mud mass transport velocity,  $U$ , is obtained as the sum of the Eulerian mass transport velocity,  $U_E$ , and the Stokes drift,  $U_S$ :

$$U = U_E + U_S \quad (13)$$

By introducing the average viscosity,  $\mu_{ave}$ , in one wave period, the Eulerian mass transport velocity is calculated from the average momentum equation:

$$\mu_{ave} \frac{\partial^2 U_E}{\partial z^2} = \frac{\partial \overline{\rho_m u^2}}{\partial x} = -2D_H \overline{\rho_m u^2} \tag{14}$$

for which the boundary conditions are

$$U_E = 0 \quad (z = 0) \tag{15}$$

$$\frac{\partial U_E}{\partial z} = 0 \quad (z = d) \tag{16}$$

The Stokes drift can be calculated by

$$U_S = \frac{\partial u}{\partial x} \int u dt = \overline{\left( -\frac{1}{C} \frac{\partial u}{\partial t} - u D_H \right) \int u dt} \tag{17}$$

**4.4 Comparison between calculation and experiment**

Four series of experiments were done for the water content ratios of 132, 171, 223 and 379 %. In each series, the mud mass transport velocity was measured for one case and the wave height distribution was measured for various incident wave periods and heights. The mud mass transport was measured by the same procedure as Sakakiyama and Bijker (1989). Figure 14 and 15 show examples of comparison between the calculated and measured wave height distribution and vertical profile of the mud mass transport velocity, respectively. Figure 16 compares the calculated and measured damping coefficients as a function of the wave period (frequency). The agreements are generally good.

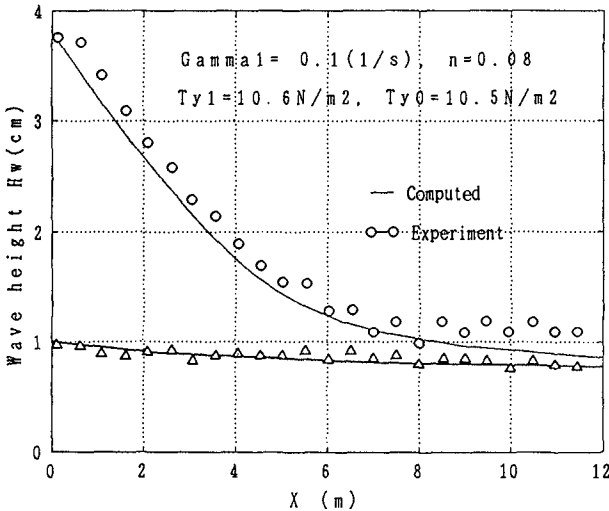


Figure 14: Comparison between calculated and measured wave damping.

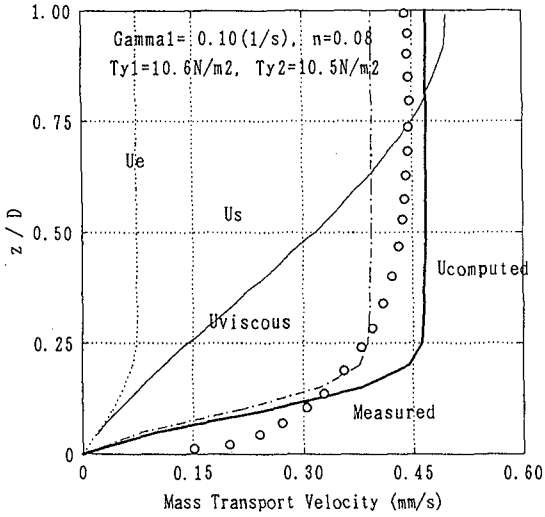


Figure 15: Comparison between calculated and measured vertical profiles of the mud mass transport velocity.

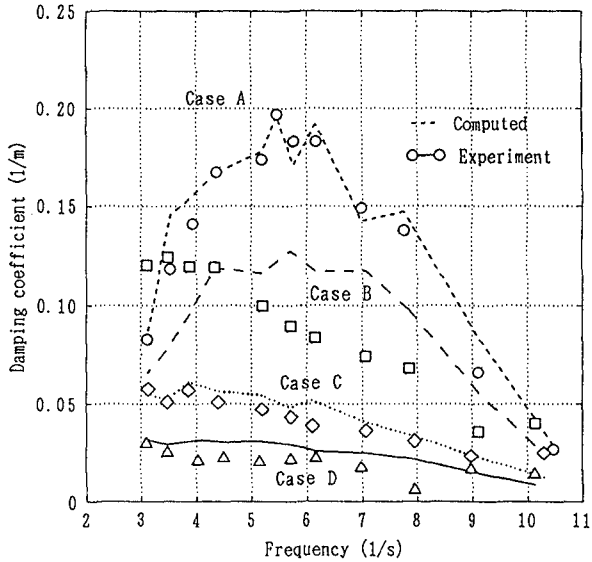


Figure 16: Comparison between calculated and measured damping coefficients.

## 5 Conclusion

The rheological properties of mud are studied by a dynamic rotary shear meter which was designed and made to measure the shear stress under an arbitrary change of shear rate. Experiments are done to confirm the predominance of the mud mass transport mode, the validity of the small amplitude wave theory for predicting wave characteristics and the predominance of the pressure as an external force of the mud motion. Based on the proposed empirical rheology model, a numerical model is developed to simulate the motion of bed mud due to wave action. Comparisons with the measurements show good agreement both for the vertical profile of the mud mass transport velocity and for the wave height damping.

In the future study, the parameters used in the rheology model should be formulated as a function of the water content ratio. In addition, bed materials other than kaolinite should be tested. In the present study, the pressure is assumed to be uniform vertically throughout the bed since its thickness is small enough. However, the vertical motion and consolidation process should be taken into account for analyzing the motion of the bed mud of a large depth.

## References

- [1] Mehta, A. J. and P.-Y. Maa (1986): Waves over mud: Modeling erosion, Proc. 3rd Int. Symp. on River Sedimentation, pp. 588-601.
- [2] Mei, C. C. and P. L.-F. Liu (1987): A Bingham-plastic model for a muddy seabed under long waves, J. of Geophys. Res., Vol. 92, No. C13, pp. 14581-14584.
- [3] Otsubo, K. and K. Muraoka (1988): Critical shear stress of cohesive bottom sediments, J. Hydraulic Eng., Vol. 114, No. 10, pp. 1241-1256.
- [4] Sakakiyama, T. and E. W. Bijker (1989): Mass transport velocity in mud layer due to progressive waves, J. of Waterway, Port, Coastal and Ocean Eng., ASCE, Vol. 115, No. 5, pp. 614-633.
- [5] Shibayama T., M. Okuno and S. Sato (1990): Mud transport rate in mud layer due to wave action, Proc. 22nd Int. Conf. on Coastal Eng., ASCE, pp. 3037-3049.
- [6] Tsuruya, H., S. Nakano and J. Takahama (1987): Interaction between surface waves and a multi-layered mud bed, Rep. Port and Harbour Res. Inst., Ministry of Transport, Japan, Vol. 26, No. 5, pp. 141-173.
- [7] Tsuruya, H., Nakano, S. and J. Takahama (1986): Investigation of rheological properties of soft muds with a rotary visco-meter, Tech. Note Port and Harbour Res. Inst., Ministry of Transport, Japan, No. 566, 29p.